# SERS-active dielectric metamaterials based on periodic nanostructures

**Andrey Lagarkov,[1] Igor Budashov,[2] Vladimir Chistyaev,[1] Alexander Ezhov,[3] Andrey Fedyanin,[3] Andrey Ivanov,[1,*] Ilya Kurochkin,[2,4] Sergey Kosolobov,[5] Alexander Latyshev,[5] Dmitriy Nasimov,[5] Ilya Ryzhikov,[1] Maxim Shcherbakov,[3] Aleksandr Vaskin,[1] and Andrey K. Sarychev[1]**

[1] *Institute for Theoretical and Applied Electrodynamics, Russian Academy of Sciences, Russia*
[2] *Faculty of Chemistry, Lomonosov Moscow State University, Russia*
[3] *Faculty of Physics, Lomonosov Moscow State University, Russia*
[4] *Emanuel Institute of Biochemical Physics, Russian Academy of Sciences, Russia*
[5] *Rzhanov Institute of Semiconductor Physics, Siberian Branch, Russian Academy of Sciences, Russia*

[*] *av.ivanov@physics.msu.ru*

**Abstract:** New dielectric SERS metamaterial is investigated. The material consists of periodic dielectric bars deposited on the metal substrate. Computer simulations as well as real experiment reveal extraordinary optical reflectance in the proposed metamaterial due to the excitation of the multiple dielectric resonances. We demonstrate the enhancement of the Raman signal from the complex of 5,5'-dithio-bis-[2-nitrobenzoic acid] molecules and gold nanoparticle (DTNB-Au-NP), which is immobilized on the surface of the barshaped dielectric metamaterial.



**OCIS codes:** (260.0260) Physical optics; (240.0240) Optics at surfaces; (240.6695) Surface-enhanced Raman scattering.

## References and links

1. M. Fleischmann, P. Hendra and A. McQuillan, "Raman spectra of pyridine adsorbed at a silver electrode," Chem. Phys. Lett. **26**(2), 163–166 (1974).
2. S. Lal, S. Link and N. J. Halas, "Nano-optics from sensing to waveguiding," Nat. Photonics **1**, 641–648 (2007).
3. B. Sharma, R. R. Frontiera, A.-I. Henry, E. Ringe, and R. P. Van Duyne, "SERS: metamerials, applications, and the future," Mater. Today **15**(1-2), 16–25 (2012).
4. F. Brouers, S. Blacher, A. N. Lagarkov, A. K. Sarychev, P. Gadenne, and V. M. Shalaev, "Theory of giant Raman scattering from semicontinuous metal films," Phys. Rev. B **55**(19), 234–245 (1997).
5. M. Fan, G. F. S. Andrade, and A. G. Brolo, "A review on the fabrication of substrates for surface enhanced Raman spectroscopy and their applications in analytical chemistry," Anal. Chim. Acta **693**, 7–25 (2011).
6. F. Hu, H. Lin, Z. Zhang, F. Liao, M. Shao, Y. Lifshitz, and S.-T. Lee, "Smart liquid SERS substrates based on $Fe_3O_4/Au$ nanoparticles with reversibly tunable enhancement factor for partical quantitative detection," Sci. Rep. **4**, 7204 (2014).
7. L. Stolcova, J. Proska, and M. Prochazka, "Hexagonally ordered gold semishells as tunable SERS substrates," in *Proceedings of 4th International Conference Nanocom*, (2012), pp. 1–6.
8. N. M. B. Perney, J. J. Baumberg, M. E. Zoorob, M. D. B. Charlton, S. Mahnkopf, and C. M. Netti, "Tuning localized plasmons in nanostructured substrates for surface-enhanced Raman scattering," Opt. Express **14**(2), 847–857 (2006).
9. B. Yan, A. Thubagere, W. R. Premasiri, L. D. Ziegler, L. D. Negro, and B. M. Reinhard, "Engineered SERS substrates with multiscale signal enhancement: nanoparticle cluster arrays," ACS Nano **3**(5), 1190–1202 (2009).
10. A. D. McFarland, M. A. Young, J. A. Dieringer, and R. P. Van Duyne, "Wavelength-scanned surface-enhanced Raman excitation spectroscopy," J. Phys. Chem. B **109**, 11279–11285 (2005);
11. M. G. Banaee and K. B. Crozier, "Mixed dimer double-resonance substrates for surface-enhanced Raman spectroscopy," ACSNano **5**(1), 307–314 (2011).

#256681 Received 4 Jan 2016; revised 1 Mar 2016; accepted 2 Mar 2016; published 24 Mar 2016

12. W.-D. Li, F. Ding, J. Hu, and S. Y. Chou, "Three-dimensional cavity nanoantenna coupled plasmonic nanodots for ultrahigh and uniform surface-enhanced Raman scattering over large area," Opt. Express**19**(5), 3925–2936 (2011).
13. N. Mattiucci, G. D'Aguanno, H. O. Everitt, J. V. Foreman, J. M. Callahan, M. C. Buncick, and M. J. Bloemer, "Ultraviolet surface-enhanced Raman scattering at the plasmonic band edge of a metallic grating," Opt. Express **20**(2), 1868–1877 (2012).
14. J.-A. Huang, Y.-Q- Zhao, X.-J. Zhang, L.-F. He, T.-L. Wong, Y.-S. Chui, W.-J. Zhang, and S.-T. Lee, "Ordered Ag/Si nanowires array: wide-range surface-enhanced Raman spectroscopy for reproducible biomolecule detection, Nano Lett. **13**(11), 5039–5045 (2013).
15. J. Lee, B. Hua, S. Park, M. Ha, Y. Lee, Z. Fan, and H. Ko, "Tailoring surface plasmons of high-density gold nanostar assemblies on metal films for surface-enhanced Raman spectroscopy," Nanoscale **6**, 616–623 (2014).
16. N. Zhang, L. Liu, Z. Liu, H. Song, X. Zeng, D. Ji, A. Cheney, S. Jiang, and Q. Gan, "Ultrabroadband metasurface for efficient light trapping and localization: a universal sufrace-enhanced Raman spectroscopy substrate for 'all' excitation wavelengths," Adv. Mater. Interfaces **2**(10), 1500142 (2015).
17. H. Xu, E. J. Bjerneld, M. Kall, and L. Borjesson, "Spectroscopy of single hemoglobin molecules by Surface Enhanced Raman Scattering," Phys. Rev. Lett. **83**(21), 4357–4360 (2009).
18. M. S. Kiran, T. Itoh, K. Yoshida, N. Kawashima, V. Biju, and M. Ishikawa, "Selective detection of HbA1c using surface enhanced resonance Raman spectroscopy," Anal. Chem. **82**(4), 1342–1348 (2010).
19. M. K. Hedayati, A. U. Zillohu, T. Strunskus, F. Faupel, and M. Elbahri, "Plasmonic tunable metamaterial absorber as ultraviolet protection film," Appl. Phys. Lett. **104**, 041103 (2014).
20. K. Liu, S. Jiang, D. Ji, X. Zeng, N. Zhang, H. Song, Y. Xu, and Q. Gan, "Super absorbing ultraviolet metasurface, IEEE Photon. Technol. Lett. **27**(14), 1539–1542 (2015).
21. Y. Han, R. Lupitskyy, T.-M. Chou, C. M. Stafford, H. Du, and S. Sukhishvili, "Effect of oxidation on surface-enhanced Raman scattering activity of silver nanoparticles: a quantitative correlation," Anal. Chem. **83**, 5873–5880 (2011).
22. P. B. Johnson and R. W. Christy, "Optical constants of the noble metals," Phys. Rev. B. **6**(12), 4370–4379 (2009).
23. G. Naik, V. Shalaev, and A. Boltaseeva, "Alternative plasmonic materials: beyond gold and silver," Adv. Mater. **25**, 3264–3294 (2013).
24. S. E. Swiontek, M. Faryad, and A. Lakhtakia, "Surface plasmonic polaritonic sensors using a dielectric columnar thin film," J. Nanophotonics **8**, 083986 (2014).
25. A. Lakhtakia and M. Faryad, "Theory of optical sensing with Dyakonov-Tamm waves," J. Nanophotonics **8**, 083072 (2014).
26. I. Avrutsky, R. Soref, and W. Buchwald, "Sub-wavelength plasmonic modes in a conductor-gap-dielectric system with a nanoscale gap," Opt. Express **18**(1), 348–363 (2010).
27. I. Avrutsky, I. Salakhutdinov, J. Elser, and V. Podolskiy, "Highly confined optical modes in nanoscale metal-dielectric multilayers," Phys. Rev. B. **75**, 241402 (2007).
28. K. V. Sreekanth, A. De Luca, and G. Strangi, "Experimental demonstration of surface and bulk plasmon polaritons in hypergratings" Sci. Rep. **3**, 3291 (2013).
29. Y.-G. Bi, J. Feng, Y.-S. Liu, Y. Chen, X.-L. Zhang, X.-C. Han, and H.-B. Sun, "Surface plasmon-polariton mediated red emission from organic light-emitting devices based on metallic electrodes integrated with dual-periodic corrugation," Sci. Rep. **4**, 7108 (2014).
30. A. K. Sarychev and V. M. Shalaev, *Electrodynamics of Metamaterials* (World Scientific, 2007).
31. S. O. Boyarintsev and A. K. Sarychev, "Computer simulation of surface enhanced Raman scattering in nanostructured metamaterials," J. Exp. Theor. Phys. **113**(6), 963–971 (2011).
32. A. V. Ivanov, A. V. Vaskin, A. N. Lagarkov, and A. K. Sarychev, "The field enhancement and optical sensing in the array of almost adjoining metal and dielectric nanorods," Proc. SPIE **9163**, 91633C1–91633C13 (2014).
33. A. I. Kuznetsov, A. E. Miroshnichenko, Y. H. Fu, J. Zhang, and B. Lukyanchuk, "Magnetic light," Sci. Rep. **2**, 492–497 (2012).
34. H. Cao and J. Wiersig, "Dielectric microcavities: model systems for wave chaos and non-Hermitian physics," Rev. Mod. Phys. **87**, 61–111 (2015).
35. R.-M. Ma, S. Ota, Y. Li, S. Yang, and X. Zhang, "Explosives detection in a lasing plasmon nanocavity," Nat. Nanotechnol. **9**, 600–604 (2014).
36. C. E. Soteropulos, H. K. Hunt, and A. M. Armani, "Determination of binding kinetics using whispering gallery mode microcavities," Appl. Phys. Lett. **99**, 103703 (2011).
37. S. I. Shopova, R. Rajmangal, S. Holler, and S. Arnold, "Plasmonic enhancement of a whispering-gallery-mode biosensor for single nanoparticle detection," Appl. Phys. Lett. **98**, 243104 (2011).
38. V. R. Dantham, S. Holler, V. Kolchenko, Z. Wan, and S. Arnold, "Taking whispering gallery-mode single virus detection and sizing to the limit," Appl. Phys. Lett. **101**, 043704 (2012).
39. A. Armani, R. Kulkarni, S. Fraser, R. Flagan, and K. Vahala, "Label-free, single-molecule detection with optical microcavities," Science **317**, 783–787 (2007).
40. T. Aoki, B. Dayan, E. Wilcut, W. P. Bowen, A. S. Parkins, T. J. Kippenberg, K. J. Vahala, and H. J. Kimble, "Observation of strong coupling between one atom and a monolithic microresonator," Nature **443**, 671–674

#256681 Received 4 Jan 2016; revised 1 Mar 2016; accepted 2 Mar 2016; published 24 Mar 2016

(2006).
41. N. Ozer, "Optical properties and electrochromic characterization of sol-gel deposited ceria films," Sol. Energ. Mat. Sol. C. **68**, 391–400 (2001).
42. P. Patsalas, S. Logothetidis, and C. Metaxa, "Optical performance of nanocrystalline transparent ceria films," Appl. Phys. Lett. **81**(3), 466–468 (2002).
43. K. C. Krogman, T. Druffel, and M. K. Sunkara, "Anti-reflective optical coatings incorporating nanoparticles," Nanotechnology **16**, s338–s343 (2005).
44. A. Verma, N. Karar, A. K. Bakhshi, H. Chander, S. M. Shivaprasad, and S. A. Agnihotry, "Structural, morphological and photoluminescence characteristics of sol-gel derived nano phase $CeO_2$ films deposited using citric acid," J. Nanopart. Res. **9**, 317–322 (2007).
45. C. Mansilla, "Structure, microstructure and optical properties of cerium oxide thin films prepared by electron beam evaporation assisted with ion beams," Solid State Sci. **11**, 1456–1464 (2009).
46. G. Balakrishnan, S. T. Sundari, P. C. Kuppusami, P. C. Mohan, M. P. Srinivasan, E. Mohandas, V. Ganesan, and D. Sastikumar, "A study of microstructural and optical properties of nanocrystalline ceria thin films prepared by pulsed laser deposition," Thin Solid Films **519**, 2520–2526 (2011).
47. T.-S. Oh, Y. S. Tokpanov, Y. Hao, W. Jung, and S. M. Haile, "Determination of optical and microstructural parameters of ceria films," J. of Appl. Phys. **112**, 103535 (2012).
48. R. Murugan, G. Vijayaprasath, T. Mahalingam, Y. Hayakawa, and G. Ravi, "Effect of rf power on the properties of magnetron sputtered $CeO_2$ thin films," J. Mater. Sci: Mater Electron **26**(5), 2800–2809 (2015).
49. M. I. Tribelsky and B. S. Luk'yanchuk, "Anomalous light scattering by small particles," Phys. Rev. Lett. **97**, 263902 (2006).
50. *Principles of Optics. Electromagnetic Theory of Propagation, Interference and Diffraction of Light*, 4th ed. (Pergamon, 1968).
51. E. C. L. Ru and P. G. Etchegoin, *Principles of Surface-Enhanced Raman Spectroscopy and Related Plasmonic Effects* (Elsevier, 2009).
52. M. Rahmani, B. Lukiyanchuk, B. Ng, A. K. G. Tavakkoli, Y. F. Liew, and M. Hong, "Generation of pronounced Fano resonances and tuning of subwavelength spatial light distribution in plasmonic pentamers," Opt. Express **19**(6), 4952–4956 (2011).
53. M. Cottat, N. Lidgi-Guigui, I. Tijunelyte, G. Barbillon, F. Hamouda, P. Gogol, A. Aassime, J.-M. Lourtioz, B. Bartenlian, and M. L. de la Chapelle, "Soft UV nanoimprint lithography-designed highly sensitive substrates for SERS detection," Nanoscale Res. Lett. **9**, 623 (2014).
54. D. Gerard and S. K. Gray, "Aluminium plasmonics," J. Phys. D: Appl. Phys. **48**(18), 1–14 (2015).
55. V. Canalejas-Tejero, S. Herranz, A. Bellingham, M. C. Moreno-Bondi, and C. A. Barrios, "Passivated aluminium nanohole arrays for label-free biosensing applications," ACS Appl. Mater. Interfaces **6**, 1005–1010 (2013).
56. E. D. Palik *Handbook of optical constants* (Elsevier Science, 1991).
57. J. Turkevich, P.S. Stevenson, and J. Hiller, "A study of the nucleation and growth processes in the synthesis of colloidal gold," Discuss. Faraday Soc. **11**, 55–75 (1955).
58. I. Kurochkin, I. Ryzhikov, A. Sarychev, K. Afanasiev, I. Budashov, M. Sedova, I. Boginskaya, S. Amitonov and A. Lagarkov, "New SERS-active junction based on cerium dioxide facet dielectric films for biosensing," Adv. Electromagn. **3**(1), 57–60 (2014).
59. M. G. Gromova, L. V. Sigolaeva, M. A. Fastovets, E. G. Evtushenko, I. A. Babin, D. V. Pergushov, S. A. Amitonov, A. V. Eremenko, and I. N. Kurochkin, "Improved absorption of choline oxidase on a polyelectrolyte LBL film in the presence of iodine anions," Soft Matter. **7**, 7404–7409 (2011).
60. U. Tamer, I. H. Boyaci, E. Temur, A. Zengin, I. Dincer, and Y. Elerman, "Fabrication of magnetic gold nanorod particles for immunomagnetic separation and SERS application," J. Nanopart. Res. **13**, 3167–3176 (2011).
61. A. H. Kupcov and G. N. Zhizhin, *The Fourier Spectra of Raman Scattering and Infrared Absorption of Polymers* (Fizmatlit, 2001).

## 1. Introduction

Manipulating light at the nanoscale using plasmonics has attracted much attention in recent years due to applications in the sub-wavelength imaging, signal processing, optical sensing etc. The excitation of the surface plasmon waves and localized plasmons at the metal surface can be used in a number of advanced applications. One of the major application is the development of the high-sensitive bio-chemical Surface Enhanced Raman Scattering (SERS) sensors [1–3]. Such sensors are based on the generation of various plasmon modes at the metal surface and further Raman scattering of the plasmons by the analyte molecules. The excited molecules generate secondary plasmons that are also much enhanced. The radiation from the secondary plasmons gives SERS signal [4]. SERS substrates typically consist of metallic clusters of gold

#256681 Received 4 Jan 2016; revised 1 Mar 2016; accepted 2 Mar 2016; published 24 Mar 2016

or silver nanoparticles embedded into a dielectric matrix. The investigated SERS signal is reported to be enhanced up to $10^2 - 10^9$ [5–16]. Thus SERS procedure allows to detect a low concentration of bio- and chemical agents. One of the exciting application is the selective detection of the glycated hemoglobin and glycated albumin in the humans blood [17, 18]. The commonly usage of such noble metals as gold and silver in plasmonic devices is associated with their small ohmic losses or high DC conductivity. The multilayer metal-dielectric SERS substrates for hot spots generation over a wide range of excitation wavelengths are investigated recently. For example dimers composed of nanorods and pairs of rings placed at the glass substrate are considered in [11]. The vertical quartz nanorods covered by gold "hats" demonstrate huge SERS enhanced factor (EF) $G \simeq 10^9$ [12]. Aluminum bars deposited on the sapphire substrate, where the analyte is deposited in the gaps between the bars, are predicted to provide the EF $G \simeq 10^9$ even in ultraviolet spectral range [13]. The periodic array of the silver-coated vertical nanowires gives EF $G \simeq 10^6$ in rather wide optical range [14]. Large local field enhancement is demonstrated by using the high-density gold nanostars assembled on the top of the very thin dielectric film (thickness $\sim 1\,nm$, which covers silver film [15]. Very recently the SERS EF $G \simeq 5 \times 10^7$ was obtained in almost all visible range in the semecontinous silver films, which is separated from the ground silver plate by the $70\,nm$ thick $SiO_2$ spacer layer [16]. It is interesting to note that the systems *metal film–dielectric spacer–metal plate* are investigated as plasmonic metamaterial super absorbers (see e.g. [16, 19, 20] and reference therein). Yet the optical response of the metals is damped due to large overall loss, which includes interband transitions, intraband transitions and additional scattering due to the defects in solids. Another disadvantage of metals in terms of plasmonic devices is the chemical instability associated with degradation in air [21]. For example, the silver nanostructures are very sensitive to sulfatization process. The gold nanostructures are more stable, however, gold has large interband loss in the blue part of the visible range for the wavelength $\lambda < 600\,nm$ [22]. The mentioned optical properties of the metals have a negative impact on the sensors operating. The novel approaches in materials providing advantages in optical device performance are discussed in [23]. The approach based on dielectric materials seems to be promising [24,25]. The excitation of different plasmon modes in the metal-dielectric multilayers have been previously investigated [26–29]. In our work we present basic metal-dielectric metamaterials, which exhibits collective dielectric resonances in microwave as well as in visible frequency range. The metamaterial is fabricated from dielectric bars placed on the metal substrate. We demonstrate surface enhanced Raman scattering (SERS) in the investigated dielectric metamaterial. The gold nanoparticles, covered by DTNB (5,5'-dithio-bis-[2-nitrobenzoic acid]) molecules, are used as indicator of the SERS phenomenon.

## 2. Field enhancement in the dielectric resonance

Let us consider the uniform dielectric layer with thickness $d$ placed on the metallic substrate in $x, y$ plane. The incident light has the electric field $\mathbf{E} = \mathbf{E}_0 \exp(ikz)$, where $k = 2\pi/\lambda$ is the wave vector, $\lambda$ is the free-space wavelength. The surface electric field, which is result of the interference of the incident and reflected waves propagating along $z$ axis, is given by the following Eq.

$$\mathbf{E}_{surface} = 2\mathbf{E}_0 \exp(-idk) / \left[1 + in\cot(dkn)\right], \tag{1}$$

where $n$ is the refractive index. The condition $d = (2m+1)\lambda/4n$ gives $\mathbf{E}_{surface} = 2\mathbf{E}_0$, where $\mathbf{E}_0$ is the incident electric field. That is the amplitude of the surface electric field is twice larger than the amplitude of the incident electric field. The value of SERS signal, described EF $G$ (see [30, 31]) is given by

$$G = \frac{\langle |\mathbf{E}_\omega(\mathbf{r})|^2 \, |\mathbf{E}_{\omega-\Delta\omega}(\mathbf{r})|^2 \rangle}{|\mathbf{E}_0|^4} \simeq \frac{\langle |\mathbf{E}_\omega(\mathbf{r})|^4 \rangle}{|\mathbf{E}_0|^4}, \tag{2}$$

#256681 Received 4 Jan 2016; revised 1 Mar 2016; accepted 2 Mar 2016; published 24 Mar 2016

where $\omega$ is the frequency of exciting radiation, $\Delta\omega$ is the frequency of the Stokes shift; the second Eq. holds for $\Delta\omega \ll \omega$. It follows from Eqs. (1) and (2) that the $G$ factor reaches its maximum $G = 16$. The SERS signal can be additionally increased by combination of plasmonic and dielectric resonators [32]. Suppose that the field enhancement is achieved at some frequency $\omega^*$ and the width of the resonance is larger than the Stokes shift $\Delta\omega$. Then it follows from Eq. (2) the effective SERS is achieved when the laser freqency $\omega$ is larger than $\omega^*$ while the frequency of the Raman line is less than $\omega^*$, i.e., the condition $\omega - \Delta\omega < \omega^* < \omega$ is fulfilled. This result was first obtained in the seminal experiment [10]. In the present paper we also consider another possibility when metal-dielectric metamaterial has two or more sharp resonances separated by $\Delta\omega_i$. Such metamaterial can be tuned for the detection of particular analytes that have the signature $\Delta\omega_i$.

Electric field enhancement in the dielectric micro particles is well known phenomenon. The electric and magnetic resonances can be excited in the almost all particles made, for example, from silica, ceria and the other dielectrics [33, 34]. Very recently tiny number of the explosive molecules was detected by semiconductor resonator in the plasmonic laser [35]. The em field enhancement in the whispering gallery resonances is used in bio and chemical sensors [36] including detecting micro-nanoparticles [37], virus [38] and, even, single molecule [39, 40]. The size of the whispering gallery resonators is typically larger than the wavelength. The electric field in the dielectric resonances could be concentrated in a hot spot, which size is much smaller than the wavelength. The local field enhancement in the spherical particle made of ceria (cerium oxide $CeO_2$), where simple dipole Mie resonance is excited, is shown in Fig. 1. Refractive index of ceria is intensively investigated in recent years [41–48]. The measured refractive index $n$ depends on the wavelength, structure of the ceria films used in the experiments [43, 44, 47], temperature [42, 46], and on the RF power of the magnetron sputtering used for the film preparation [48]. The index is typically larger for the more dense ceria films, so we take ceria index $n \simeq 2.3$ for the mono-crystal particles discussed below.

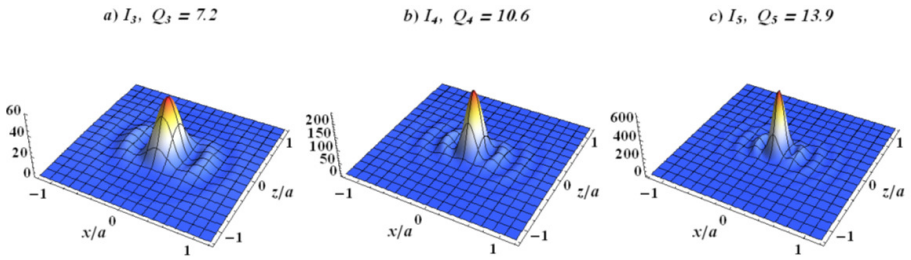


Fig. 1. Electric field distribution $I_m = |E/E_0|^2$ and $Q_m$ factor in dipole free oscillations in ceria spherical particle of radius $a = 400\,nm$ ; dipole directed along "$z$" axis: a) Radial "quantum" number $m = 3$, $\lambda_3 = 716\,nm$; b) Radial "quantum" number $m = 4$, $\lambda_4 = 507\,nm$; c) Radial "quantum" number $m = 5$, $\lambda_5 = 393\,nm$.

We consider the natural em field vibration that is an eigenmode. When the dipole mode is excited, which radial "quantum" number $m_r > 3$ the em field concentrates in the center (Fig. 1). The maximum of the electrical field, which is much larger than the ambient field, could be estimated in the following way. We take into account that the em field decays during the free oscillations due to the radiation loss. The energy outflow from the particle approximates as $S_e \sim a^2|E_0|^2$, where $a$ is the radius of the dielectric sphere, $E_0$ is the ambient electric field. In the dipole resonance on the order $m$ the field intensity $I_m = |E_m|^2$ concentrates in the hot spot in the center of the particle (see Fig. 1). The radius of the hot spot estimates as $r_m \sim a/m$, therefore, the energy outflow $S_m$ from the hot spot is $S_m \sim r_m^2 I_m$. We neglect, for simplicity, the

#256681 Received 4 Jan 2016; revised 1 Mar 2016; accepted 2 Mar 2016; published 24 Mar 2016

small ohmic loss and equating the energy flows $S_e$ and $S_m$ obtaining $I_m \sim E_0^2 m^2$. That is the field maximum is $m^2$ times larger than the outside field as it is shown in Fig. 1. Note that we consider here the situation when the radiative dumping prevails over the dissipative loss similar to [49].

For the further esteem let us consider the field distribution in the electric dipole Mie resonance, excited in the dielectric sphere of the radius $a$ [33, 50]. The sphere with permittivity $\varepsilon = n^2$ is placed in the origin of the coordinates. The permittivity of the outer space is chosen to be equal to one. The electromagnetic field oscillates with resonance frequency $\omega$, wave vector $k = \omega/c$. We use the spherical symmetry of the problem to introduce the vector potential for the inside field

$$A_{\mathrm{i}z} = iE_0 \frac{a\sin(u)}{2nu_a\, u f(u_a)}, \tag{3}$$

which is directed along $z$ axis, where the dimensionless coordinate $u = knr$, $r = \sqrt{x^2+y^2+z^2}$, $u_a = kna$ and the function $f$ is defined as $f(u) = (u\cos u - \sin u)/u^3$. It is convenient to introduce spherical coordinates $\{r, \theta, \varphi\}$. Then magnetic and electric fields inside the sphere are

$$\mathbf{H}_{\mathrm{i}}(u,\theta) = \mathrm{curl}\,\mathbf{A}_{\mathrm{i}} = -iE_0 \left\{0, 0, \frac{uf(u)}{2nf(u_a)}\sin\theta\right\}, \tag{4}$$

$$\mathbf{E}_{\mathrm{i}}(u,\theta) = \frac{i}{\varepsilon k}\mathrm{curl}\mathbf{H}_{\mathrm{i}} = E_0 \left\{\frac{{u_a}^3 f(u)}{n^2u^3 f(u_a)}\cos\theta, \frac{{u_a}^3\left[f(u)+u^2\sin u\right]}{2n^2u^3 f(u_a)}\sin\theta, 0\right\}, \tag{5}$$

that is magnetic field has $\varphi$ component only and rotates around $z$ axis.

The outside electromagnetic field is given by the vector potential

$$A_{\mathrm{e}z} = E_0\,\frac{au_a^2}{2u\,(u_a+in)}\exp\left[ik(r-a)\right], \tag{6}$$

which is chosen in such a way that the boundary conditions $H_{\mathrm{i}\varphi}(a) = H_{\mathrm{e}\varphi}(a) = -iE_0u_a\sin\theta/(2n)$ and $\varepsilon E_{\mathrm{i}r}(a) = E_{\mathrm{e}r}(a) = E_0\cos(\theta)$ are automatically accomplished. The third boundary condition $E_{\mathrm{i}\theta}(a) = E_{\mathrm{e}\theta}(a)$ gives the dispersion Eq. for the resonance frequencies

$$(u_a+in)\sin u_a - u_a f(u_a)\left[\left(n^2-1\right)u_a - in\left(u_a^2-n^2+1\right)\right] = 0 \tag{7}$$

in terms of $u_a = kna$. Let us consider the large radial numbers $m \gg 1$ when the dimensionless frequency $u_a \gg 1$. Then the asymptotic solution of Eq. (7) has the following form.

$$u_m = \pi m - \frac{\pi}{2} - \frac{1}{\pi m} - \frac{1}{2\pi m^2} - i\left(\mathrm{arccoth}\,n + \frac{n+\mathrm{arccoth}\,n}{\pi^2 m^2}\right), \tag{8}$$

which works surprisingly good for $m > 2$. Note the eigen frequencies of the considered free osculations $\omega_m = kc = cu_m/na$ are complex and have non-vanishing imaginary part since the eigenmodes decays due to the radiation loss. From Eq. (8) we obtain the quality factor $Q_m = -\mathrm{Re}\,u_m/(2\mathrm{Im}\,u_m)$, for the considered dipole resonances:

$$Q_m = \frac{\pi\left(2\pi^2m^3 - \pi^2m^2 - 2m - 1\right)}{4\left[(\pi^2m^2+1)\mathrm{arccoth}\,n + n\right]}, \tag{9}$$

for $m > 2$ and $n > 1$. Thus we obtain that the simple dielectric structure could give strong field concentration.

Suppose that analyte molecules are injected in the slit made in the spherical dielectric particle as it is shown in Fig. 2. Then the enhancement $G$ of the Raman scattering, which is proportional

#256681 Received 4 Jan 2016; revised 1 Mar 2016; accepted 2 Mar 2016; published 24 Mar 2016

to $\langle|E|^4\rangle$, is estimated as $G \sim I_m^2 E_0^{-4} \sim Q^4 \sim (mn)^4$. Therefore SERS in dielectric structures could be compared with SERS in the plasmonic structures. Yet, the dielectric structures has the distinguish property to enhance the fields at some characterisic frequencies as it is shown in Fig. 1. Note that in the case of the planar dielectric metamaterials, discussed in the next sections, the local electric field also concentrates in gaps between the dielectric features (cf., Fig. 2 and 4).

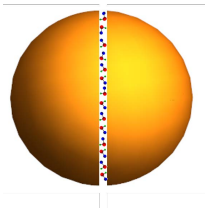

Fig. 2. Slotted spherical dielectric particle with an analyte.

The Raman signal typically has few characteristic spectral lines shifted in respect to the laser frequency $\omega$ by the so-called Stokes shifts $\Delta\omega_i \ll \omega$ [51]. The dielectric resonator, which has set of the closely packed resonances $\omega_i$, can be used as a sensor for particular substances when the resonances frequencies coincide with Raman spectral lines $\omega_i = \omega + \Delta\omega_i$. That is the gaps between the dielectric resonances coincide with the Stokes shifts. Since the dielectric resonances are well localized in the space (see Fig. 1), we can split the resonances in the simplest way, by placing two particles in close vicinity to each other. Let us consider two dielectric spheres that are placed at "z" axis with the distance $d$ between their centers. Suppose that dipole resonances are excited in the particles. The set of the eigenmodes can be classified by the direction of the vector potential $\mathbf{A}_\mathrm{i}$, (see Eq. 3). There are three independent eigenmodes $A_x, A_y$ and $A_z$. It is safe to neglect the interaction of the orthogonal modes. Interaction energy $\Delta U$ of the aligned dipole modes, which are supposed to be synchronized by an external field, is estimated as $\Delta U_m \sim P_m^2/d^3$, where $P_m$ is the dipole moment of the $m$ eigenmode so that $P_m^2 \sim \varepsilon^2 I_m r_m^6$. The ratio between interaction energy $\Delta U$ and the eigenmode energy $\varepsilon I_m r_m^3 \sim \varepsilon I_m (a/m)^3$ gives the frequency split $\Delta\omega \sim \varepsilon (r_m/d)^3 \sim \varepsilon (a/d)^3 m^{-3}$ due to the resonance interaction. Typically the Stokes shifts are tens – hundreds times smaller than the laser frequency. Therefore, the close packed dielectric spheres could exhibit properly resonance shifts and can be used for the SERS sensors.

The plasmon resonances that are excited in the small cluster of metal nanoparticles were considered in [52], M. Rahmani *et al.* The metal particles, organized in the regular pentagon demonstrates two low $Q$ resonances separated by $\Delta\lambda$ which is larger than hundred nanometers ($\Delta\omega > 5 \cdot 10^3\, cm^{-1}$). Therefore such plasmonic structures hardly could be used as SERS sensors. We believe that the proper designed dielectric structures can give the resonances corresponding to the Raman lines and allow to designed effective SERS sensors for detecting the desired analyte. The resonances in the regular dielectric structures are consider below.

## 3. Thin periodic dielectric films

### *3.1. Optic resonances*

In this section we consider the periodic array of dielectric bars 1 and 2 (see Fig. 3) with different height $h_{1,2}$, width $d_{1,2}$, and distance between them $d_s$ that are placed at the metal substrate 3. We consider the case of $p$-polarization, where the electric field $E_0$ of the incident em wave is $y$ directed.

#256681 Received 4 Jan 2016; revised 1 Mar 2016; accepted 2 Mar 2016; published 24 Mar 2016

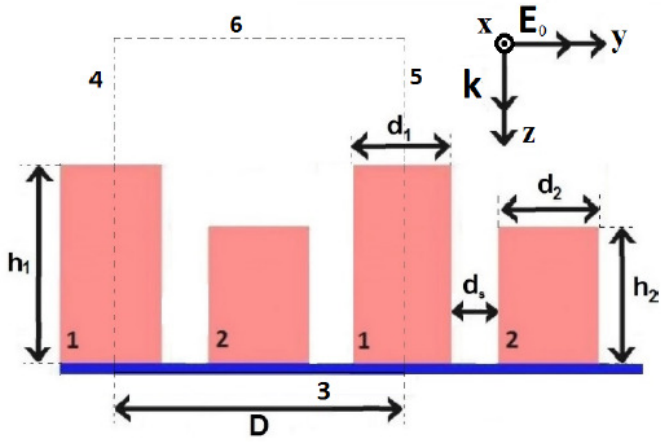


Fig. 3. Periodic dielectric bars; period of unit cell – $D$; parameters are: $d_{1,2}$ – width, $h_{1,2}$ – height, inter-bar distance – $d_s$, $E_0$ – incident electric field, $k$ – wave number of incident wave.

The em field distribution in the periodic dielectric bars, placed on the metal substrate, is modeled in the COMSOL environment. The Helmholtz Eq. was solved by finite element method (FEM). The metal substrate 3 is modeled as a perfect conductor. In actual experiment the substrate can be made from gold, silver or aluminum [53–55]. As the dielectric material ceria ($CeO_2, \varepsilon = 5.3 + 0.02\,i$) was chosen. The dielectric bars can be made of material with high dielectric constant, for example, polymethyl methacrylate ($PMMA,\ \varepsilon = 2.2$), titanium dioxide ($TiO_2,\ \varepsilon = 5.5$), silicon ($Si,\ \varepsilon = 15$) etc. [28]

The thickness of thin-films is varied $h_{1,2} = 0.1 \sim 1\mu m$; the period $D$ in $x$ direction is about $D = 0.5\,\mu m$. Figure 4 demonstrates electric field distribution $|E/E_0|$ ($E_0$ - is the incident field) for resonances excited at the free-space wavelengths $\lambda = 0.97\mu m$ and $\lambda = 0.57\mu m$. It can be seen that modes shown in Fig. 4 have a different nature. The left mode ($\lambda = 0.97\mu m$) describes the surface dielectric resonance while the right one ($\lambda = 0.57\mu m$) excites due to dielectric resonance (interference of incident and reflected fields) as we mentioned in the previous section.

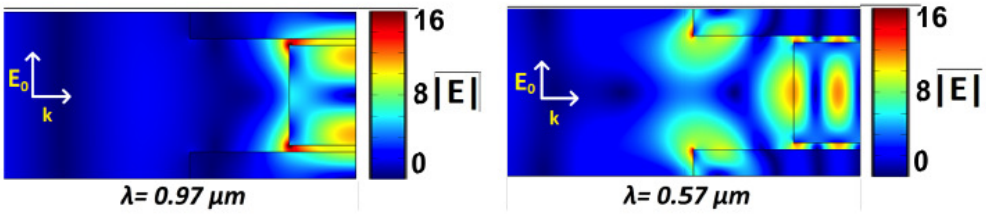


Fig. 4. Electric field distribution $|E/E_0|$ for a) $\lambda = 0.97\,\mu m$, b) $\lambda = 0.57\,\mu m$ in the unit cell shown in Fig. 3; parameters of the material are: $h_1 = 0.5\,\mu m$, $h_2 = 0.2\,\mu m$, $d_1 = 0.16\,\mu m$, $d_2 = 0.3\,\mu m$, $d_s = 0.02\,\mu m$, $D = 0.5\,\mu m$, $\varepsilon = 5.3 + 0.02\,i$.

The Raman enhancement $G$ and the reflectance for the proposed dielectric metamaterial are shown in Figs. 5(a) and 5(b). As we expect the resonance peaks of intensity in $G$ spectrum correspond to the minima of reflectance. The frequency of surface resonances is defined by the period $D$ of the system while the frequency of the dielectric resonances is defined by the thicknesses of the film $h_1$ and $h_2$. It is remarkable that the frequencies of excitation of the different

#256681 Received 4 Jan 2016; revised 1 Mar 2016; accepted 2 Mar 2016; published 24 Mar 2016

modes can be independently tuned. Note that we deal with mainly dielectric resonances since the metal substrate is considered to be made from the perfect conductor, which does no support surface plasmons and any other surface waves.

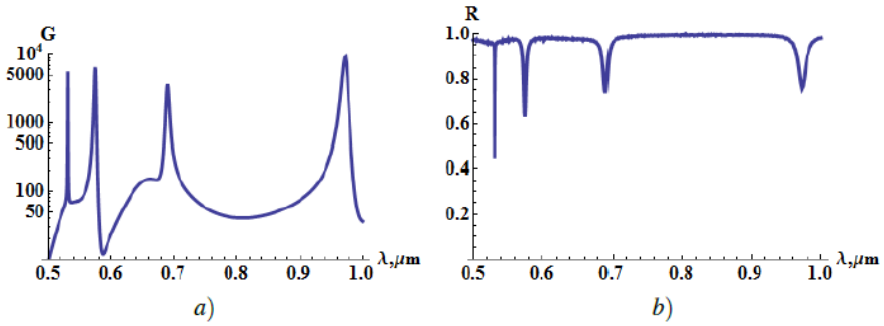


Fig. 5. a) Enhancement of Raman signal $G$. b) Reflectance $R$ as a function of free-space wavelength $\lambda$; Parameters of structure are: $h_1 = 0.5\,\mu m$, $h_2 = 0.2\,\mu m$, $d_1 = 0.16\,\mu m$, $d_2 = 0.3\,\mu m$, $d_s = 0.02\,\mu m$, $D = 0.5\,\mu m$, $\varepsilon = 5.3 + 0.02\,i$.

### 3.2. *Microwave dielectric metamaterial*

Dielectric metamaterials, in contrast to the plasmon counterparts, has no intrinsic frequency. Therefore, its properties can be investigated in microwave after the proper scaling. We study the excitation and the interference of the surface waves in the simplest microwave structure, presented in Fig. 6. In the first case the periodic dielectric bars, fabricated from the usual window glass, were placed on the glass plate, and then on the aliminium substrate. The microwave permittivity of the glass $\varepsilon(f = 9.042\,GHz) = 6.83(\pm 0.5\%) + 0.1\,i(\pm 20\%)$ was measured in East-Siberian branch of All Russia Research Institute of Physicotechnical and Radio-Engineering Measurements by Dr. E.U. Tokareva. We also investigate all-dielectric films without the metal substrate.

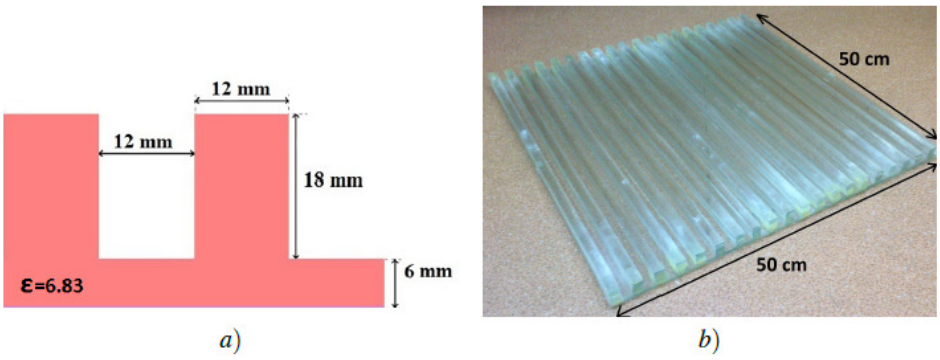


Fig. 6. Periodic dielectric bars used for microwave experiment; geometric parameters are: $d_1 = d_2 = 12mm$, $h_1 = 6mm$, $h_2 = 18mm$, $d_s = 12mm$, $\varepsilon = 6.83 + 0.1i$.

Figure 7 demonstrates predicted (orange line) and measured (red line) reflectance for the bar shaped dielectric metamaterial for $p$- and $s$-polarization at the microwave frequencies. The minima in the reflectance spectrum correspond to the frequencies of excitation of the dielectric

#256681 Received 4 Jan 2016; revised 1 Mar 2016; accepted 2 Mar 2016; published 24 Mar 2016

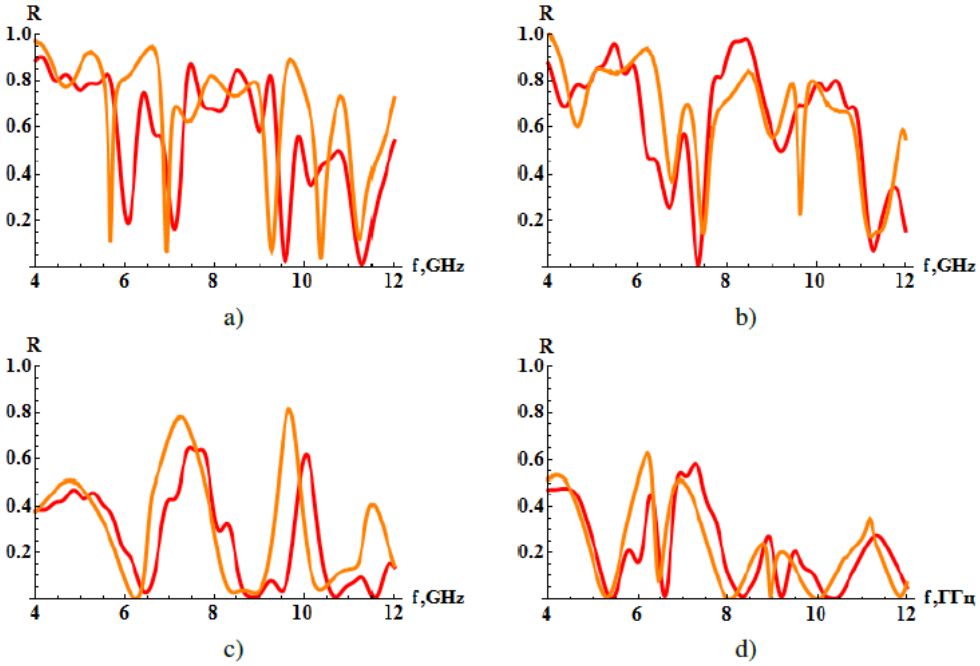


Fig. 7. Simulated (orange line) and measured (red line) reflectance for glass bars placed on the metal substrate: (a) *p*-polarization, (b) *s*-polarization; the same without the metal substrate: (c) *p*-polarization, (d) *s*-polarization.

resonances, where electric field is much enhanced (Figs. 8 – 10). Figures 8(b) and 9(b) demonstrate the coordinate-dependence electric field distribution $|E/E_0|$ ($E_0$ amplitude of incident field) at the resonance frequencies for p- wave polarization in both two cases - with glass bars placed on metal substrate and without metal substrate. The important point is that the giant electric field concentrates outside the glass bars near air-dielectric boundary and reaches the maxima when wavelength become comparable to the period of the structure. The experimental results are in an agreement with computer simulations. The frequency dependence of the reflectance $R(f = \omega/2\pi)$ is similar for the materials with and without metal substrate. Yet, the enhancement of the electric field in the case of dielectric bars with metal substrate has the larger value due to the reflection from the metal.

#256681 Received 4 Jan 2016; revised 1 Mar 2016; accepted 2 Mar 2016; published 24 Mar 2016

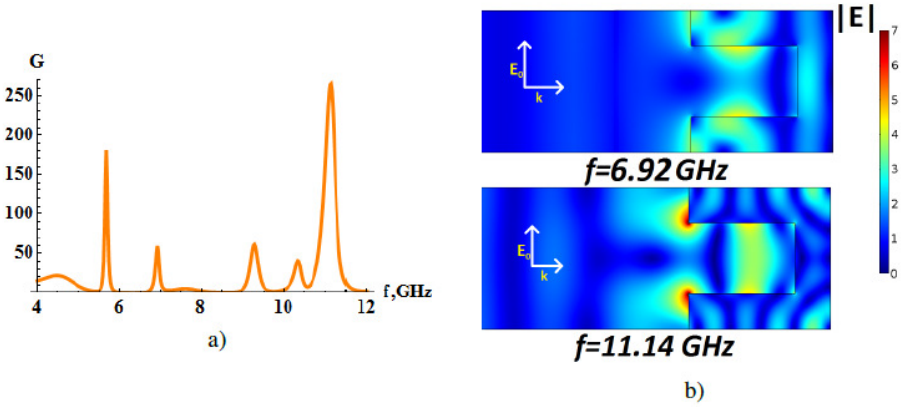


Fig. 8. (a) Enhancement $G$ for glass bars placed on metal substrate for $p$-polarization. (b) Electric field distribution $|E/E_0|$ ($E_0$ – amplitude of incident field) for resonance frequencies f=6.92 GHz and f=11.14 GHz: red color corresponds to the maximum amplitude of the electric field.

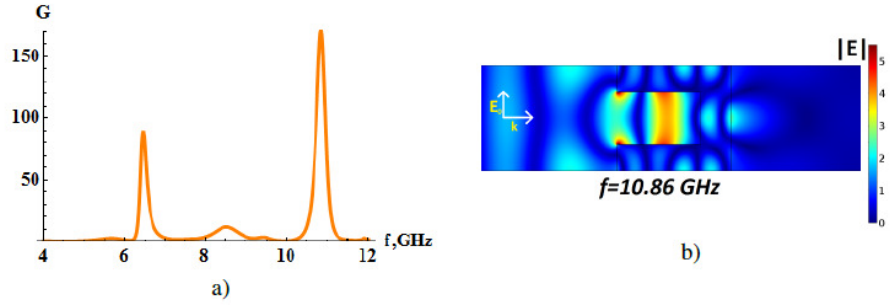


Fig. 9. (a) Enhancement $G$ for glass bars without substrate for $p$-polarization. (b) Electric field distribution $|E/E_0|$ ($E_0$ – amplitude of incident field) for resonance frequency $f = 10.86\,GHz$.

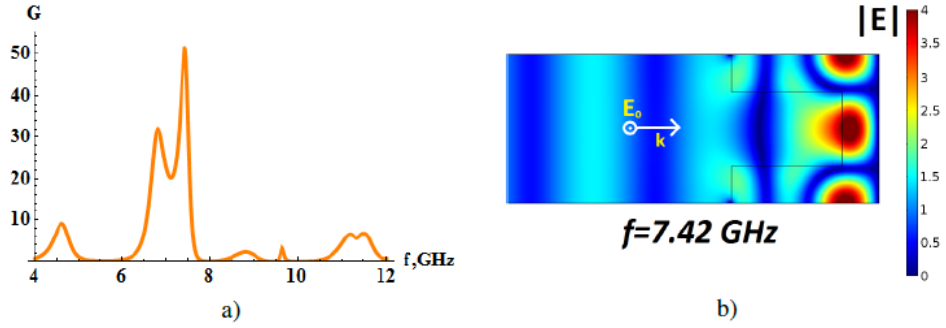


Fig. 10. (a) Enhancement $G$ for glass bars placed on metal substrate for $s$-polarization. (b) Electric field distribution $|E/E_0|$ ($E_0$ - amplitude of incident field) for resonance frequency f=7.42 GHz.

#256681 Received 4 Jan 2016; revised 1 Mar 2016; accepted 2 Mar 2016; published 24 Mar 2016

The resonances for the *p*- and *s*-polarization have different frequencies, which gives an additional opportunity for the fitting to the resonace frequencies for a particular analyte. When our microwave experiment confirmed the computer simulations we begin fabrication and investigation of the optical dielectric metamaterials. First experimental results are discussed in the next section.

### *3.3. Dielectric plasmons*

The computer model of the metamaterial investigated in Sec. 3.1 was further modified to take into account optical properties of the real metal substrate. The height of the bars is the same $h_1 = h_2$ (see Fig. 3). The metamaterial is made of polymethyl methacrylate (*PMMA*) on the silver substrate. The reflectance has a minima in the wavelength region from $600\,nm$ to $1000\,nm$, shown in Fig. 11(b). The local electric field at the resonance is shown in Fig. 11(a) ($\lambda = 785nm$). It should be mentioned that the resonance frequency which is located at the wavelength $\lambda = 785\,nm$ corresponds to high-usage lasing wavelength. Figure 11 demonstrates the excitation of both two resonances - plasmon and dielectric.

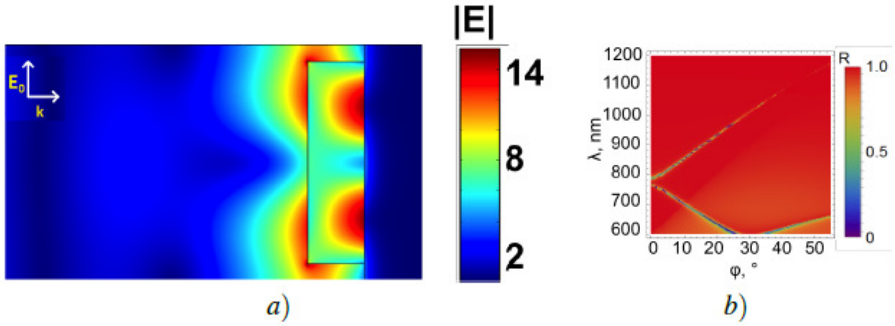


Fig. 11. (a) The electric field distribution $|E/E_0|$ ($E_0$ - amplitude of incident field) at the resonance wavelength $785\,nm$, *p*-polarization, normal incidence ($\phi = 0$); geometric parameters are: $h_1 = h_2 = h = 140\,nm$, $d_1 = d_2 = d = 500\,nm$, $d_s = 100\,nm$, $n = 1.485$. (b) Reflectance as function of angle of incidence (with respect to normal) and free-space wavelength $\lambda$.

## 4. Optical dielectric metamaterial

### *4.1. Fabrication*

We prepared the metal-dielectric composite metamaterial, which consists of the silicon substrate, thick gold layer and periodic bars of *PMMA* (Fig. 12). The metamaterial was fabricated on Si(100) surface by means of electron-beam lithography technique. The sample with size of $(10 \times 10 \times 0.3\,mm)$ were cut from n-type of silicon wafer doped by phosphorus with resistivity of $0.3\,\Omega \cdot cm$. After wet-chemical cleaning in petroleum ether, the sample was rinsed in deionized water. Subsequently the 40-nm gold film was deposited on the silicon sample having a native oxide layer covered by 4 nm pre-layer of titanium by means of magnetron sputtering in ultrahigh vacuum conditions. A focused-ion-beam (FIB 1540XB, Carl Zeiss, Germany) cutting technique has been successfully applied to measuring the thickness of the deposited metallic layer. The sample was covered by single layer of polymethyl methacrylate (PMMA). PMMA thin film was prepared by spin coating from the toluene solution onto the surface of a silicon sample in order to produce a film between $600\,nm$ and $1200\,nm$ thick. Average resist film thicknesses were measured using standard ellipsometry technique. An electron beam with a diameter about $1\,nm$ has been used for structuring the surfaces of the sample. Lithography operation was

#256681 Received 4 Jan 2016; revised 1 Mar 2016; accepted 2 Mar 2016; published 24 Mar 2016

provided by means of Raith-150 ultrahigh-resolution e-beam tool (Raith, Germany). The 350-nm-wide lines and spaces have been fabricated in PMMA layer using electron-beam exposure of $(100 \times 100\,\mu m)$ surface area.

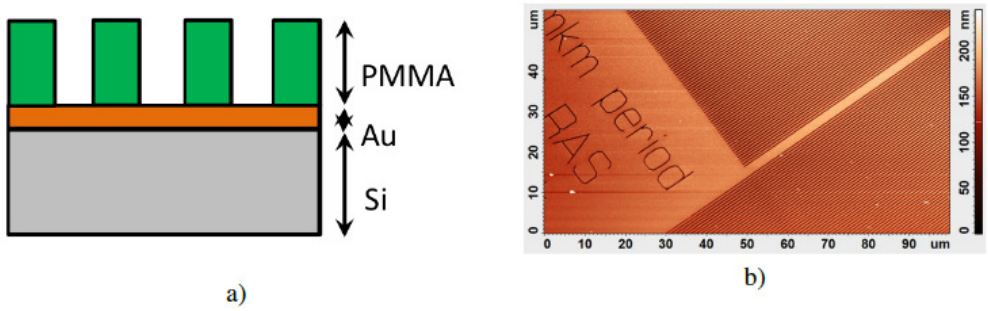


Fig. 12. (a) Periodic dielectric structure based on Au and PMMA. (b) Atomic force microscopy (AFM) of periodic dielectric structure: period $670 - 680\,nm$, Au thickness $40\,nm$, PMMA thickness $1700\,nm$.

### *4.2. Measurements*

The layer thicknesses were determined using spectroscopic ellipsometer UVISEL 2 (Horiba Jobin Yvon) equiped by software DeltaPsi2 (Horiba Jobin Yvon). The same ellipsometer was used for the measurements of reflectance spectra. The period of the structure and direction of the grating vector was determined by atomic force microscope (AFM) images analysis. AFM images were obtained by the scanning probe microscope NTEGRA Prima (NT-MDT). Silicon cantilevers NSG10 (NT-MDT) were used. Measurements were performed in semicontact mode. Measurements of reectance spectra carried out with rectangular eld aperture, which limits the size of the light spot on the sample surface to minimize the contribution of the unstructured regions of the sample. The size of these spots that are listed to the angle of incidence of 70 degrees were $(120 \times 182)\mu m^2$ or $(220 \times 250)\mu m^2$. The spot size on the sample was chosen to maximize the signal to noise ratio. Change of aperture was caused by the fact that one of the spot size on the sample dependent on the angle of incidence.

Measurement of local reflection spectra of *p*- and *s*-polarized light (Rp and Rs) was carried out by measuring the reflectance spectrum of unpolarized light (R) and spectra of ellipsometric angles $\Psi$ and $\Delta$. Rp and Rs are calculated based on the measured values. Measurement modes are selected from those that are provided in the software. The selection was due to the fact that during the measurement of spectra R, $\Psi$ and $\Delta$ polarization of incident light is constant, whereas in the measurement of Rp and Rs polarization of incident light is changed during the measurement. Since the polarization of the incident light is determined by the angular position of polarizing Rochon prism, the change in the direction of the polarization is due to the rotating prism. This turn leads to a shift of the light spot on the sample. Since we carry out measurements using a beam spot size of about 100 microns, such displacement of the spot on the sample can lead to measuring Rp and Rs with the surface offset relative to each other. We measure the reflectance spectra of the structured area and reflectance spectra of the unstructured, flat region of the layered structure. For example, the signals from the areas $x < 20$ and $x > 50$ in Fig. 11 are compared.

It should be noted that plasmonic resonances supported by metal nanostructures are limited by the incident angle. Moreover, consistently with planar technology, optical-device designers prefer normal incidence because of practical convenience. We use approach based on excitation of combined metal-dielectric plasmons. The inclusion of dielectric structures on the metal

#256681 Received 4 Jan 2016; revised 1 Mar 2016; accepted 2 Mar 2016; published 24 Mar 2016

surface allow to excite both plasmon resonance at the metal surface and dielectric resonance in the case of normal incidence. Therefore, the cascade effect of the EM enhancement is occur.

### *4.3. Optical properties*

We use the results of the numerical simulations as well as real experiment to compare the reflectance spectra of the structured area of periodic bars with the reflectance spectra of the unstructured, flat region of the layered structure. The calculations and measurements are done for the wide spectrum of angles from 35 to 70 degrees (with respect to normal) for *p*- (blue line) and *s*-polarization (red line) of incident field (Fig. 13). The approximation for Au for calculations was taken from experimental results [22,56]. The results for narrow range of angles (35-40 degrees) are presented in Figs. 14 and 15, which demonstrate an agreement of theory and experiment. The narrow range was chosen due to curve dips in this region. It should be noted that we cannot reach the excitation of plasmon resonances due to large thickness of PMMA layer (approximately 1700 nm) but the system exhibits collective dielectric resonances. The disagreement between calculations and measurements in *s*-polarization reflectance (red dashed line - measurements, red solid line - theory) shown in Fig. 15 can be explained by specific features of beam aperture of the measurement equipment.

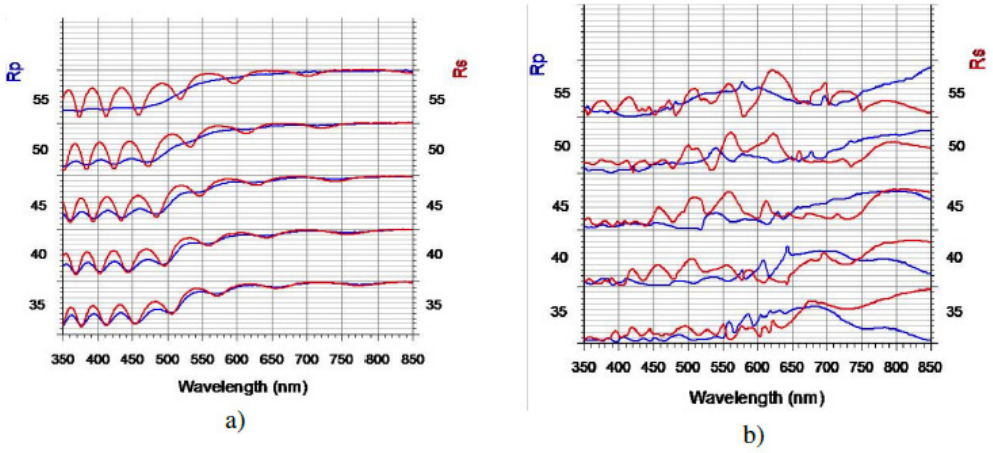


Fig. 13. (a) Experimental reflectance from multilayer film, which consists of Au and PMMA layers neighboring the structured area. (b) Experimental reflectance from PMMA stripe-shaped structure; blue lines *p*-polarization, red lines *s*-polarization.

#256681 Received 4 Jan 2016; revised 1 Mar 2016; accepted 2 Mar 2016; published 24 Mar 2016

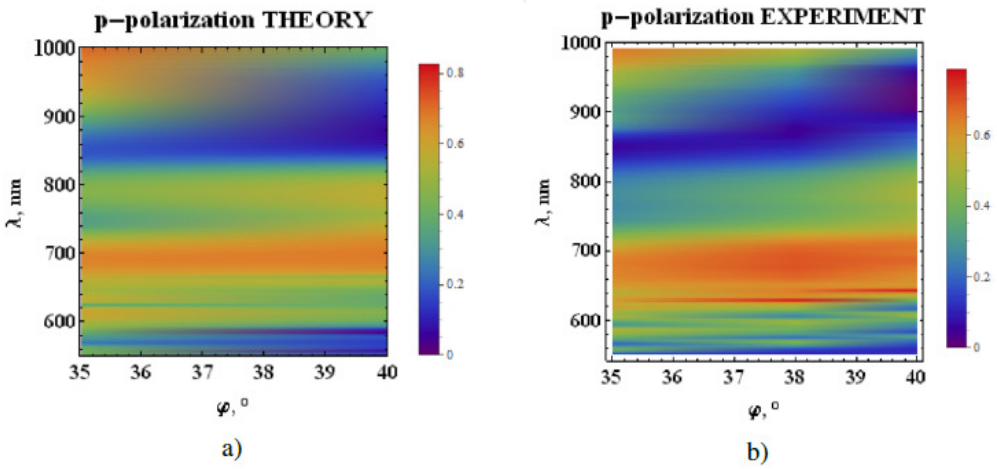


Fig. 14. (a) Simulated and (b) Measured reflectance for *p*-polarization for different angles of incidence and wavelengths; blue color corresponds to minima of reflectance.

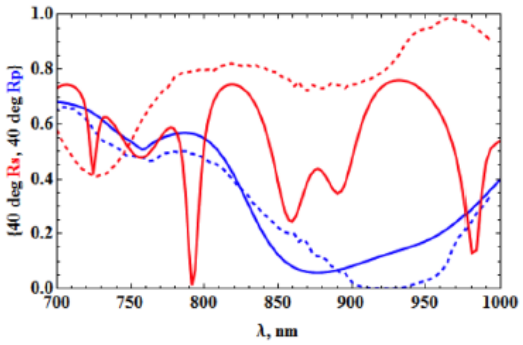


Fig. 15. Simulated (solid line) and measured (dashed line) reflectance for *p*- (blue) and *s*- (red) polarization.

## 5. Raman signal enhancement in dielectric metamaterials

### *5.1. Preparation and immobilization of gold nanoparticles on the bar-shaped metamaterial*

Au-nanoparticles (Au-NP) were prepared by well-known citrate method [57]. Au-NP size was determined by Nanoparticle Tracking Analysis (average size - $56 \pm 1\,nm$ ) with using "Nanosight LM10" equipment ("Nanosight Ltd.", UK). For the preparation of SERS active particles, Au-NPs were covered by semicontinuous monolayer of 5.5-dithio-bis(2-nitrobenzoic acid) - (DTNB) molecules in accordance to [58] with some modifictations. The solution of Au-NP was twice diluted by DTNB solution in HEPES (5 mM, pH 8 at 25° C). Incubation was performed overnight at room temperature. Then, a solution of PEG in water (10 mg/ml) was added to a concentration of 0.5 mg/ml and incubated for 30 min. Solution was centrifuged (1300 rev/min, 10 min), the supernatant was poured, the precipitate was resuspended in water with PEG (0.5 mg/ml) to the concentration of the nanoparticles equal to the initial one. Maximum absorption spectrum of the sol was shifted from 534 to 540 nm.

The conjugate Au-NP-TNB was adsorbed onto bar shaped metamaterial after deposition of

#256681 Received 4 Jan 2016; revised 1 Mar 2016; accepted 2 Mar 2016; published 24 Mar 2016

polycation (poly(diallyldimethylammonium chloride)) according to the procedure described in the article [59] with some modifications. The sample was incubated in a solution of PDDA (10 mg/ml) in water (prepared at least a day before use) for 20 min. Then washed with water (3 times 300 $\mu$l) and dried by air flow. Further drop of 5 $\mu$l conjugate Au-NP-TNB in water (optical density of $\approx$ 0.1) were applied to the area of the periodic dielectric bars modified PDDA, and incubated for 1 hour at room temperature in a humid chamber (the substrate surface was horizontal). Then washed with water (3x300 $\mu$l) and dried by air flow.

We estimate that 60% of the surface of Au-NP is covered by DTNB. The conjugate of Au-NP with DTNB (Au-NP-DTNB) has series of well defined Raman peaks and can be used as a SERS indicator [60].

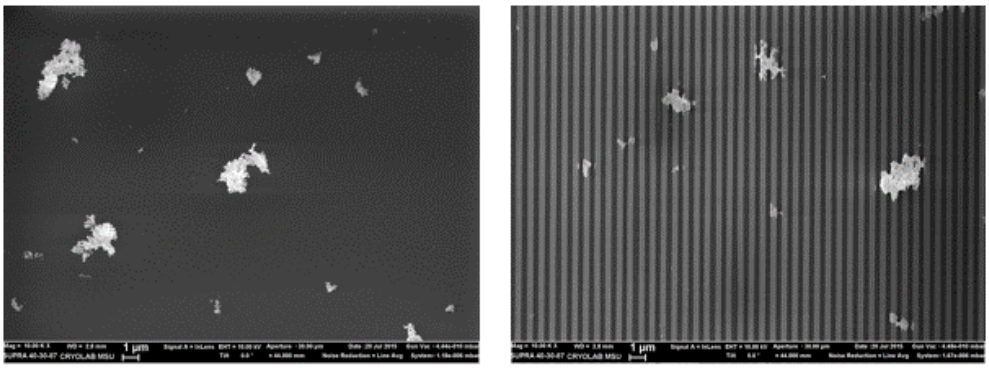

a) b)

Fig. 16. SEM images of Au-NP-DTNB deposited on *PMMA* layer (a) Flat, unstructed area (b) Bar shaped PMMA metamaterial, cf. Fig. 12.

Morphology of bar-shaped metamaterial after Au-NP deposition were studied by SEM using a Supra-40 microscope (Carl Zeiss, Germany). Representative SEM images are shown in Fig. 16.

### *5.2. Raman signal*

A Raman spectrometer innoRam, model BWS445 (B)-785S (B&W Tek, Inc. USA) with continuous-wave laser-785 was used for the collection of spectra using an excitation wavelength of 785 nm. The excitation was performed in an epi configuration through a 20X objective (NA= 0.4) on a microscope. Laser power for the experiment was 29 mW.

The Raman spectra of PMMA was registered at the lines $810\,cm^{-1}$, $598 cm^{-1}$, acquisition time was 5 seconds. The Raman signal fron Au-NP-DTNB conjugate was registered at the Stocks shifts of DTNB [60], which are $926\,cm^{-1}$, $1060\,cm^{-1}$, $1338\,cm^{-1}$, and $1558\,cm^{-1}$. In this case acquisition time was 0.5 seconds. SERS signal intensity of these bands was calculated as the average of the measurements in the several points of the sample after subtracting the baseline signal. We compare the Raman scattering from Au-NP-DTNB conjugate deposited on the flat PMMA layer and on the bar shaped metamaterial shown in Figs. 12b and 16 to estimate SERS EF due to the dielectric metamaterial. The fraction of the surface, which is occupied by the gold nanoparticles, was estimated from SEM images with using "Gwyddion" software.

### *5.3. Results*

It was shown that the Raman spectrum of surface area includes lines $810 cm^{-1}$ and $598 cm^{-1}$ that correspond to general lines of PMMA [61]. The Raman spectrum of PMMA (without any

#256681 Received 4 Jan 2016; revised 1 Mar 2016; accepted 2 Mar 2016; published 24 Mar 2016

Au-NP) in structured area (blue line) and unstructured area (red line) is shown in Fig. 17. The intensity of Raman peak $810\,cm^{-1}$ reaches the value $110 \pm 8$ a.u. which corresponds to the flat region while the Raman peak is about $286 \pm 15$ a.u. in the structured region.

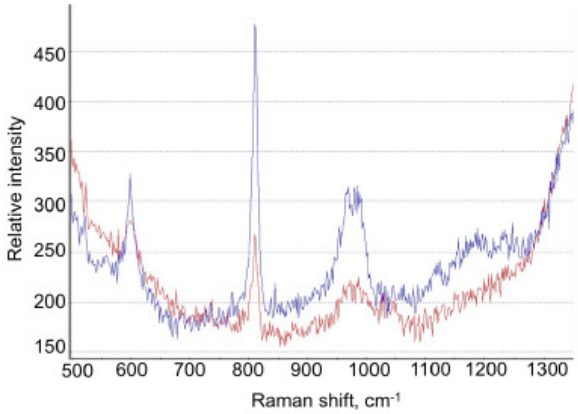


Fig. 17. Raman spectrum of *PMMA* metamaterial; blue line corresponds to the structured area, red line corresponds to flat layer of *PMMA* on the gold substrate.

The fraction of surface occupied by the gold nanoparticles estimated as a $(2.8 \pm 0.7)\%$ - in the flat region, $(4.0 \pm 1.9)\%$ - in the bar shaped region. The SERS spectrum of Au-NP-DTNB into the structured surface is shown in Fig. 18. It can be seen from Table 1 that the intensity of Raman signal for Au-NP-DTNB for Stokes shift $1338cm^{-1}$ and $1558cm^{-1}$ more than 5 times larger in case of structured area with respect to flat film.

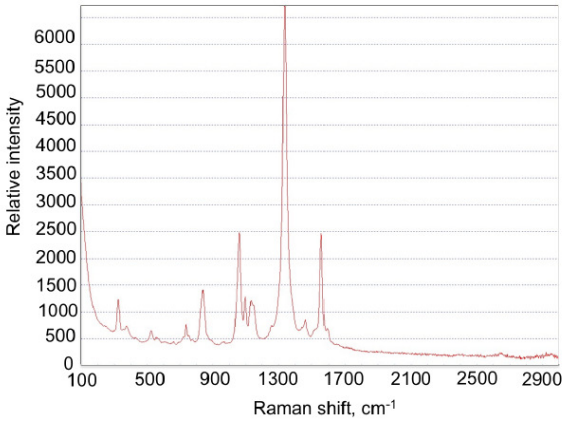


Fig. 18. SERS signal at different Raman scattering bands from Au-NP-DTNB on the structured surface after normalization to the amount of gold nanoparticles.

## 6. Conclusion

The bar-shaped metamaterial was theoretically and experimentally investigated. We used theoretical methods as well as experimental measurements (both in microwave and optical frequencies) to demonstrate the excitation of surface multiple dielectric resonances. The dielectric

#256681 Received 4 Jan 2016; revised 1 Mar 2016; accepted 2 Mar 2016; published 24 Mar 2016

Table 1. The intensity of Raman peaks of conjugate Au-NP-DTNB on the surface, a.u. (normalized to the amount of gold nanoparticles)

| | $326 cm^{-1}$ | $1060 cm^{-1}$ | $1338 cm^{-1}$ | $1558 cm^{-1}$ |
|---|---|---|---|---|
| **Enhancement** | **2.45** | **3.6** | **5.2** | **5.6** |
| Unstructured area | $162 \pm 36$ | $338 \pm 38$ | $825 \pm 97$ | $222 \pm 37$ |
| Structured area | $397 \pm 44$ | $1224 \pm 153$ | $4278 \pm 510$ | $1253 \pm 155$ |

resonances can be explained as interference of reflected and incident fields. The combination of plasmon and dielectric resonances allow to reach additional enhancement of SERS signal. The results of our analytical and numerical calculations are in a good agreement with the experimental results. The bar-shaped metamaterial was modified by Au-NP-DTNB conjugates. The intensity of Raman signal from Au-NP-DTNB for the Stokes shifts $1338\,cm^{-1}$ and $1558\,cm^{-1}$ is more than 5 times larger in case of bar structured area with respect to flat layer of the same *PMMA* material.

Note that the structure of the investigated metamaterial is far away from the optimal for SERS. It was a test sample to demonstrate the technology. Yet, we immediately achieve the Raman enhancement in Au-NP-DTNB complex as well as in PMMA dielectric. We speculate that it is the experimental evidence that SERS effect could take place in dielectric microstructures without involving any metal nanoparticles. The proposed metamaterials can be a core of the high sensitive optical sensing devices. The resonance frequencies can be tuned by variation of the shape and arrangement of the dielectric elements.


## Acknowledgments

The work was partially supported by Russian Science Foundation (RSF) (grant 16-14-00209).


#256681 Received 4 Jan 2016; revised 1 Mar 2016; accepted 2 Mar 2016; published 24 Mar 2016